TRACKING OF VORTICES IN A TURBULENT BOUNDARY LAYER

G.E. Elsinga, C. Poelma, J. Westerweel
Laboratory for Aero & Hydrodynamics
Delft University of Technology
Leeghwaterstraat 21, 2628CA Delft, The Netherlands
g.e.elsinga@tudelft.nl

A. Schröder, R. Geisler
Institut für Aerodynamik und Strömungstechnik
Deutsches Zentrum für Luft- und Raumfahrt,
Bunsenstrasse 10, 37073 Göttingen, Germany

F. Scarano
Department of Aerospace Engineering
Delft University of Technology
Kluyverweg 1, 2629HS Delft, The Netherlands

ABSTRACT

The motion of spanwise vortical elements has been tracked in the outer region between wall-normal distance $z/\delta = 0.11$ and 0.30 of a turbulent boundary layer at $Re_\theta = 2460$. The experimental dataset of time-resolved three-dimensional velocity fields used has been obtained by tomographic particle image velocimetry. The tracking of these structures yields their respective average trajectories as well as the variations thereof, quantified by the root-mean-square of the trajectory coordinates as a function of time. It is demonstrated that the variation in convection can be described by a dispersion model for infinitesimal particles in homogeneous turbulence, which suggests that these vortical structures are transported passively by the external velocity field without significant changes in their topology, at least over the present observation time of $1.2\delta/U_e$. It is shown that the measured variation in convection velocity can further be used successfully to predict the temporal development of space-time correlation functions starting from the instantaneous correlation map. In this prediction the structures are assumed to convect without change, following our observations.

1. INTRODUCTION

The convection velocity of coherent flow structures in wall-bounded turbulence has received considerable attention, first of all because of a fundamental interest in the dynamic behaviour of these structures. The turbulent flow contains a variety of structures (for a recent survey see Adrian 2007), which, in principle, may all advect at different velocities. We may then further imagine that such a difference in convection velocity ultimately causes the structures to change their relative position and interact, which results in topological changes, like for instance the generation of a new structure. In that sense convection can be seen as an appropriate starting point for the investigation of coherent structure dynamics.

Unfortunately very little quantitative information is available on the changes in convection velocity from one structure to the next, as most attention has been paid to their average convection velocities. However, as will be shown in this paper, the variation around the mean is of significant importance too, particularly when interpreting space-time correlations and assessing the validity of Taylor's hypothesis. Therefore, the aim of the present paper is to provide such quantitative information by tracking individual structures in the outer layer of a turbulent boundary layer.

Before proceeding, the main conclusions from earlier work will be summarized, which mainly concerns the average convection. First of all, the average has been shown to be scale-dependent. Kim and Hussain (1993) consider the propagation velocity of turbulent fluctuations in turbulent channel flow at different spatial wavelengths and find that it increases with spanwise scale in the near wall region. Compared to earlier experimental work (e.g. Wills 1964, Bradshaw 1967, Willmarth and Wooldridge 1962), Kim and Hussain (1993) have benefited from the introduction of direct numerical simulations (DNS), which resolves both the time and length scales in contrast to the experimental methods available at that time, such as hot-wire anemometry. The latter provide time series in a limited number of points (usually two). Therefore, the resulting space-time correlations from those experiments cannot distinguish well between a fast large eddy and slow moving small eddy.

The average convection velocity has also been found to depend on the flow variable or coherent structure under consideration (Guezennec, Piomelli and Kim 1989, Krogstad, Kaspersen and Rimestad 1998, Kim and Hussain 1993).

Furthermore, convection of the flow structures connects to some very important practical applications such as establishing the most appropriate velocity scale when converting temporal into spatial scales using Taylor's hypothesis of frozen turbulence (Taylor 1938). The validity and the interpretation of the results obtained in this way are both long-standing topics, which have been revived recently (Dennis and Nickels 2008, Del Alamo and Jimenez 2009, Moin 2009) in light of the energetic very-large-scale motions observed in Taylor reconstructions of hot-wire time signals (e.g. Kim and Adrian 1999).

As recognized before in the papers cited, there exists some variation in the instantaneous convection velocity even between coherent flow structures of the same type. This scatter has not been quantified extensively yet, but its presence is visible, for instance, in the sample probability density function for the time delay between detected events at two streamwise locations, as presented by Krogstad, Kaspersen and Rimestad (1998) in their figure 6. Furthermore, the width of the rim in the turbulent spatio-temporal power spectrum (figure 2 in Moin 2009) illustrates that a single spatial wave is associated to a range of temporal frequencies, that is a range of convection velocities (assuming the spatial wave remains undistorted).

The purpose of the present paper is to provide a further quantification of the variation in the instantaneous convection velocities of coherent structures. This will be based on the detection and tracking of large numbers of individual spanwise vortex elements in the logarithmic and outer region of a turbulent boundary layer, as described in §3. These structures are believed to be representative features for wall-bounded turbulence, especially in the context of the hairpin-type models (Adrian 2007). The resulting trajectories yield the average, but more importantly, also the root-mean-square (RMS) convection over time (§4). Furthermore, it will be demonstrated that the present results can be used to predict the space-time correlation function of different flow variables, given their respective instantaneous spatial auto-correlation functions (§5). This provides insight on how these correlations should be interpreted and puts the present results in relation to some of the earlier work, which have relied on such space-time correlations to establish average convection velocities and explore the validity, or range of applicability, of Taylor's hypothesis. In this investigation, existing three-dimensional and time-resolved experimental velocity data were used, the details of which are presented in §2.

2. EXPERIMENTAL DATASET

The turbulent boundary layer data was obtained from a time-resolved tomographic Particle Image Velocimetry measurement (Elsinga et al. 2006) in a water tunnel. The setup and first results have been described in detail by Schröder et al. (2011). Furthermore, the data were used before to study the dynamic evolution and lifetimes of the invariants of the velocity gradient tensor, which characterize the local flow topology around a fluid particle (Elsinga and Marusic 2010). For completeness, however, we will briefly recall some of the boundary layer properties here. The zero-pressure gradient boundary layer develops over a 2.5 m long flat plate with an elliptical leading edge at a free-stream flow velocity U_e of 0.53 m/s and with a free-stream turbulence level below 0.5%. Transition is forced 15 cm downstream of the elliptical leading edge by a zig-zag strip. At the measurement location, 2.0 m downstream, the boundary layer thickness δ is 37 mm and the Reynolds numbers Re_θ and Re_τ are 2460 and 800 respectively.

The three-dimensional velocity distribution $\boldsymbol{V}(x,y,z,t)$ is evaluated in an effective volume spanning $1.8\delta \times 1.8\delta$ in streamwise (x) and spanwise (y) direction and covering $0.11 < z/\delta < 0.30$ in wall-normal (z) direction in five time-series of 2 seconds each. The sampling frequency is 1 kHz corresponding to $70U_e/\delta$ and $\Delta t^+ = 0.47$, which indicates that the flow is well resolved in time. Between subsequent velocity volumes, the flow structures advect by approximately 10 wall units. The spatial resolution, taken as the cross-correlation volume linear dimension, is 0.07δ, corresponding to approximately 58 wall units in each direction, which is sufficient to capture energy containing motions in the flow (Schröder et al. 2011, Elsinga and Marusic 2010). Furthermore, 75% cross-correlation volume overlap is used in both space and time. The latter is the result of a time stepping method (correlating the volumes corresponding to first image 1 with that from the 5th image recorded 4 ms later, then image 2 with 6 and so on), which increases the dynamic range of the measurement.

The vortical structures within the measurement domain were detected by a local evaluation of the velocity gradients (see section 3), which were obtained by a second order regression filter in space and time (Elsinga et al. 2010). The frequency response of this filter is similar to the inherent window averaging effect in PIV when taking the filter kernel size equal to the cross-correlation window.

3. VORTEX DETECTION & TRACKING METHOD

The individual snapshots contain a variety of three-dimensional vortical structures and before following them in time, first a detection method is required to locate individual events. In this paper, the focus will be on spanwise vortex elements, which are defined as regions of positive spanwise swirling strength $\lambda_{ci,y}$. The detected features may not be an isolated structure, but can be part of a larger vortex. For example, a hairpin vortex contains a spanwise vortex element, i.e. the head, with quasi-streamwise vortex elements on either side, i.e. the so-called legs. The spanwise swirling strength used here, is the absolute value of the imaginary part of the eigenvalue of the reduced velocity gradient tensor J_{uw}, given by:

$$J_{uw} = \begin{bmatrix} \frac{\partial u}{\partial x} & \frac{\partial u}{\partial z} \\ \frac{\partial w}{\partial x} & \frac{\partial w}{\partial z} \end{bmatrix} \qquad (1)$$

which considers only the components in the streamwise, wall-normal plane. The eigenvalue $\lambda_{ci,y}$ is non-zero only when the velocity vectors in that plane describe a local swirling motion (Christensen and Adrian 2001). Previous investigations using Linear Stochastic Estimation (LSE) have indicated that $\lambda_{ci,y}$ is associated to the head of a hairpin type vortex (e.g. Christensen and Adrian 2001, Elsinga et al. 2010). Hairpins are a very prominent feature in the models for wall-bounded flow (see for example Adrian 2007), which has been a main motivation for choosing spanwise swirling strength. An additional reason is that it is more spatially compact than swirling in the other directions (associated with the legs of hairpins), hence easier to detect and track accurately.

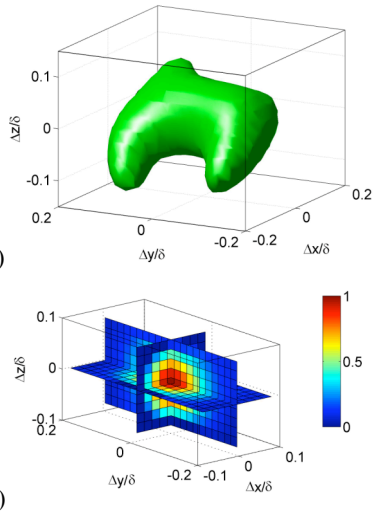

Figure 1. (a) Conditional eddy of the average flow associated to a spanwise swirling event at $z/\delta = 0.2$ wall-normal distance. The iso-surface indicates vortical motion revealed by the Q-criterion. (b) Spanwise vortex template derived from the conditional eddy, which is used for detection of spanwise vortex elements. The color-coding indicates the spanwise swirling strength normalized by the peak value.

The first step is then to create a template of the feature to be detected. For this purpose, the conditional eddy resulting from a LSE is used. It is determined by a cross-correlation of the velocity fluctuations with a specified event, which in this case is the spanwise swirl $\lambda_{ci,y}$. The present LSE calculation is analogous to the ones by Christensen and Adrian (2001) and Elsinga et al. (2010). As expected, the resulting eddy resembles a hairpin-like vortex. From the conditional eddy we take again the magnitude of the spanwise swirling strength and use that for the template (figure 1). The template has a shape that is slightly elongated in the spanwise direction, and corresponds to the head of the conditional eddy.

Structures are subsequently detected by finding the local maxima in the map resulting from a cross-correlation of the template with the measured instantaneous spanwise swirling strength distribution. The location of each maximum can be obtained to a higher, sub grid-scale, precision by performing a local Gaussian peak fit in all three directions. The peak of the fitted function is taken as the location of the identified vortex structure.

Once the spanwise vortices have been identified in the instantaneous volumes, they can be tracked in time using methods similar to those for tracking tracer particles in Particle Tracking Velocimetry (e.g. Lüthi et al. 2005). When tracking a structure, its location at the next time step is first estimated based on the local average flow velocity. If a structure can be detected at this next time instant within a specified search radius from the estimated position (by the method described above), a link is established and the new location is added to the structure's trajectory. The procedure is repeated until the structure leaves the measurement domain or no structure is detected within the search radius (0.04δ in each direction, which is smaller than the typical distance between detected structures). Approximately 85% of the detected structures can be tracked over one or more time steps in this way. The other structures must be considered spurious, since the structures should reappear at least once due to the high temporal resolution. To reduce the noise in the final trajectories, a regression filter is applied, in which a second order polynomial in time is fitted to each spatial coordinate over a window of 31 time steps (that is 31 ms corresponding to $\Delta t^+ = 15$ or $0.44\delta/U_e$). For this one-dimensional filter the cut-off wavelength is approximately equal to the window (see the appendix in the paper by Elsinga et al. 2010). A smaller window of 11 time steps was also tried yielding similar results, but with more noise.

For further analysis we consider here only the clearly detectable and tractable structures, which are not too close ($>0.07\delta$) to the borders of the measurement domain as the structure detection method by cross-correlation may not be sufficiently accurate there. Hence, only events at a distance between 0.11δ and 0.30δ from the wall are considered. Reliable detection is established by requiring that the cross-correlation coefficient during structure detection is above 0.5 (averaged over the trajectory), while traceability requires that a structure can be traced over more than 100 time steps corresponding to a convection distance of about 1.2δ.

Some examples of the resulting trajectories are given in figure 2, with superposed the corresponding detected vortex structures at its start and end. The first structure (figure 2a) is a typical arch vortex in the lower part of the measurement domain (its legs are cut at the edge of the measurement domain). In the other two examples (figures 2b and 2c), the detected event is a spanwise element connected to a larger vortex element, which extends beyond the measurement domain and is inclined with respect to the wall. The spanwise vortex elements in figures 2a and 2b do not display an appreciable change over time, while in 2c the spanwise element starts as a thin bridge between to neighboring taller structures and then thickens over time, which is due to an increase in swirling strength. The final result of the outlined tracking procedure is a total of 392 of such spanwise vortex trajectories (figure 3).

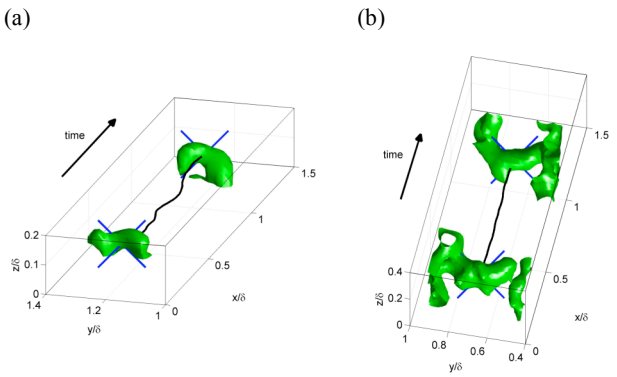

Figure 2. Three examples of spanwise vortex element trajectories (black lines) with corresponding extended vortex structure (green, iso-surface of constant Q) at the start and end of their trajectory, which are marked by the blue crosses.

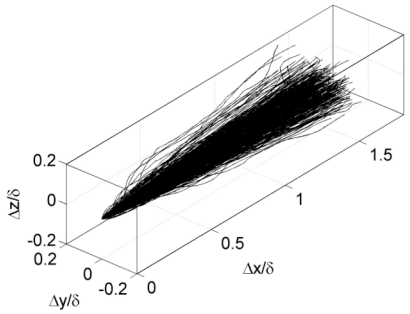

Figure 3. Trajectories of 392 detected spanwise vortex elements. The spatial coordinates are relative to the initial position of the vortex.

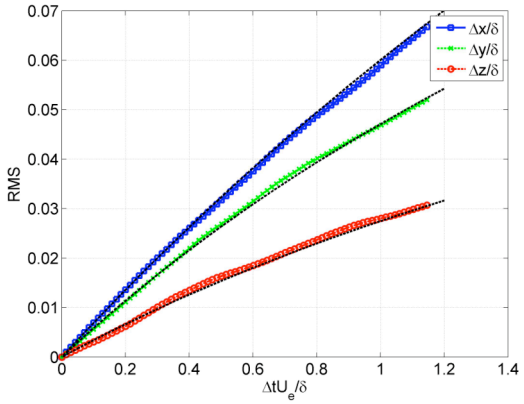

Figure 4. Spreading of the vortex trajectories in figure 3, as represented by the RMS of the relative positions $\Delta x, \Delta y, \Delta z$ versus time (symbols). The dashed black lines are fits of Taylor's (1921) model for turbulent dispersion of infinitesimal particles (Eq. 2), which suggest the observed spreading of the vortices can be described well by such a dispersion process up to at least $\Delta t U_e/\delta = 1.2$.

4. DISPERSION OF VORTICES

The spanwise vortex element tracks (figure 3) reveal a significant spreading relative to the mean convection. The average convection velocity of similar structures in a boundary layer and channel flow has already received considerable attention in the literature (e.g Del Alamo and Jimenez 2009, Krogstad et al. 1998, Kim and Hussain 1993), and the tracking results just lend additional support for the earlier observations. The average convection velocity inferred from the tracks is constant over the considered time period and equal to $0.78U_e$ in the streamwise direction (equal to the local mean flow velocity at a distance of 0.2δ from the wall), $0.06U_e$ in the wall-normal direction and zero in the spanwise direction. As already mentioned in the introduction, the mean is not the main interest here, but rather the variations around the average.

The spreading of structures is expressed in terms of the RMS of the trajectory position as a function of time, which is shown in figure 4. The results show that the RMS of the streamwise position grows fastest followed by the spanwise and wall-normal position.

Moreover, the curves are reminiscent of dispersion for infinitesimal particles in homogenous turbulence, which for the streamwise component is given by (Taylor 1921, Tennekes 1979):

$$\sigma_x^2(t) = 2\,\overline{u_c'^2}\,T_L\left[t - T_L\left(1 - e^{-t/T_L}\right)\right] \qquad (2)$$

where σ_x is the RMS of the streamwise position, u_c' is the streamwise convection velocity fluctuation, T_L is the Lagrangian integral time scale and t is time. Indeed Eq. 2 fits the results well as shown in figure 4. The fitted values used for the Lagrangian time scale and the RMS convection velocities are listed in table 1. It appears that the Lagrangian time scale for the streamwise dispersion is larger than for the other two directions, which suggests changes in the streamwise convection velocity of a given structure are relatively slow. Furthermore, when looking at the RMS convection velocity fluctuations (table 1), it is found that the streamwise and wall-normal components are only slightly lower than the RMS flow velocity fluctuations. The spanwise component, however, is about 20% larger than the flow velocity fluctuations, meaning that the spanwise vortex elements experience greater movements along its axis than what may be expected based on

the flow velocity alone. The goodness of the fit in figure 4 demonstrates that the motion of spanwise vortices in a boundary layer can be considered as a basic turbulent diffusion process up to at least a convection distance of 1.8δ (the size of the present measurement domain). To some extent this may be expected, since the characteristic time-scale for local flow topology evolution is much larger (a convection distance of about 11δ, Elsinga and Marusic 2010). Hence, the topology and spanwise vortices are not expected to undergo significantly changes within the present observation length, and consequently they experience predominantly convection, which is what has been observed.

Table 1: Fit parameters Lagrangian integral time scale T_L and RMS convection velocity components u_c', v_c', w_c' in the dispersion model (Eq. 2) for the spanwise vortex elements. For comparison the RMS flow velocities u', v', w' measured at a distance of 0.20δ from the wall are included.

direction	T_L $[\delta/U_e]$	RMS u_c', v_c', w_c' $[U_e]$	RMS u', v', w' $[U_e]$
Streamwise, σ_x	1.0	0.070	0.071
Spanwise, σ_y	0.6	0.060	0.050
Wall-normal, σ_z	0.6	0.035	0.038

5. PREDICTION OF SPACE-TIME CORRELATIONS

The present results suggest that the flow structures mainly convect without significant change over a time of $1.2\delta/U_e$. This observation can be used to predict the space-time correlation of turbulent signal, as shown below.

Consider a turbulent signal containing the turbulent eddies. From here on, we use the streamwise velocity distribution $u(\boldsymbol{x},t)$ as an example, but other quantities (like the invariants of the velocity gradient tensor) are equally possible. Then the eddy shape can be characterized statistically by the instantaneous auto-correlation function $A_{uu}(\boldsymbol{s})$:

$$A_{uu}(\boldsymbol{s}) = \frac{1}{N}\sum_{\boldsymbol{x},t} u(\boldsymbol{x},t)u(\boldsymbol{x}+\boldsymbol{s},t) \qquad (3)$$

where N is the number of samples. Assuming that the eddies do not evolve in time and are simply convected by a constant velocity $\boldsymbol{u}_c$, then $u(\boldsymbol{x},t) = u(\boldsymbol{x}+\boldsymbol{u}_c\Delta t, t+\Delta t)$, which can also be written as a convolution:

$$u(\boldsymbol{x},t+\Delta t) = \int u(\boldsymbol{x}-\boldsymbol{r},t)\delta(\boldsymbol{r}-\boldsymbol{u}_c\Delta t)d\boldsymbol{r} \qquad (4)$$

where δ is the Dirac delta function. The hairpin tracking results, however, indicate that the convective velocity is not a constant. Allowing for these variations in the convective trajectories $\boldsymbol{r}(\Delta t)$ according to a probability density function $P(\boldsymbol{r},\Delta t)$ (still assuming a pure convection without any eddy evolution), the expected velocity distribution at time $t+\Delta t$ is given by:

$$u(\boldsymbol{x},t+\Delta t) = \int u(\boldsymbol{x}-\boldsymbol{r},t)P(\boldsymbol{r},\Delta t)d\boldsymbol{r} \qquad (5)$$

or in discrete form:

$$u(\boldsymbol{x},t+\Delta t) = \sum_{r} u(\boldsymbol{x}-\boldsymbol{r},t)P(\boldsymbol{r},\Delta t) \quad \text{with} \quad \sum_{r} P(\boldsymbol{r},\Delta t) = 1 \qquad (6)$$

Subsequently, the space-time correlation $R_{uu}(\boldsymbol{s},\Delta t)$ for non-evolving eddies can be estimated as:

$$\begin{aligned} R_{uu}(\boldsymbol{s},\Delta t) &= \frac{1}{N}\sum_{\boldsymbol{x},t} u(\boldsymbol{x},t)u(\boldsymbol{x}+\boldsymbol{s},t+\Delta t) \\ &= \sum_{r}\frac{1}{N}\sum_{\boldsymbol{x},t} u(\boldsymbol{x},t)u(\boldsymbol{x}+\boldsymbol{s}-\boldsymbol{r},t)P(\boldsymbol{r},\Delta t) \\ &= \sum_{r} A_{uu}(\boldsymbol{s}-\boldsymbol{r})P(\boldsymbol{r},\Delta t) \end{aligned} \qquad (7)$$

The space-time correlation is a convolution of the instantaneous auto-correlation A_{uu} with the probability density function $P(\boldsymbol{r},\Delta t)$ representing a statistical description of the convection and spreading rate of the eddies (figure 4). The function $P(\boldsymbol{r},\Delta t)$ will be approximated by a Gaussian distribution with the RMS given by the dispersion model (table 1). A comparison with the actually measured distribution function suggests that the approximation is appropriate.

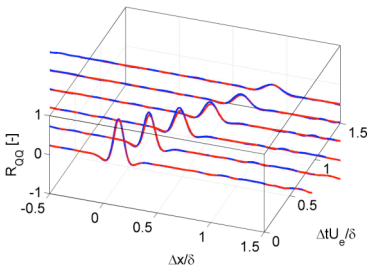

Figure 5. Predicted (red) and measured (blue) space-time auto-correlation $R_{QQ}(\Delta x,\Delta y,\Delta z,\Delta t)$ of the second invariant of the velocity gradient tensor Q, plotted along $\Delta y = \Delta z = 0$. The prediction is based on the instantaneous auto-correlation function $R_{QQ}(\Delta x,\Delta y,\Delta z,\Delta t = 0)$ and uses the observed spreading rate of the flow structures (figure 4) to predict the temporal development.

Eq. 7 has been evaluated to predict the space-time correlation R_{QQ} for the second invariant of the velocity gradient tensor Q (figure 5). The distribution $P(\boldsymbol{r},\Delta t)$ for the spanwise vortex elements (table 1) was used in this case. The prediction is found to follow both the broadening and decreasing of the correlation peak with time, which further

supports the underlying assumptions of passive eddy convection.

The decrease in the correlation peak height over time was used in the past to validate or disprove Taylor's hypothesis. The present results indicate that this decrease can be attributed to the dispersion of flow structures rather than any actual change in topology. Therefore, the hypothesis may still be useful in studying certain aspects of turbulence (e.g. the nature of the flow topology does not change significantly), even though the correlation peak may drop considerably. This drop will be stronger for the small scales, first of all because their correlation peak is narrow compared to the spreading rate of the flow structures, but also due to this spreading rate being larger than for the large-scales.

A word of caution may be added to the last point. Recently, Schröder et al. (2011) have suggested that specific, strong events can undergo visible topological change within a time period of $0.8\delta/U_e$. While their reported time evolution of conditional averages for strong vorticity and ejection events reveal only slight changes in the inclination angle, which they explained by the variation in convection velocity with wall-normal distance (consistent with what we propose here), a rapid transformation is reported for the strong sweep events. Such strong sweep events are rare, however, and contribute only marginally to the overall correlations presented in this paper.

6. CONCLUSIONS

Spanwise vortex elements were tracked in time in the outer layer of a turbulent boundary layer. The following points summarize the main conclusions:

(i) The average spanwise vortex element trajectory corresponds to the local average flow velocity, while the RMS track position can be characterized as dispersion of infinitesimal particles in homogenous turbulence (Eq. 2).

(ii) Assuming the vortical structures predominantly convect without interaction or significant topological change, the space-time correlations for different flow variables can be predicted based on their instantaneous auto-correlation and their spreading rate (i.e. the probability density function of their track position in time). This was illustrated for the second invariant of the velocity gradient tensor, Q. The prediction describes well the decrease and broadening of the correlation peak in time (at least up to the present observation time, $1.2\delta/U_e$). These temporal changes in the correlation must, therefore, be attributed mostly to the dispersion of flow structures rather than any actual change in topology.

Future work will include the tracking of larger scales of motion, the bulges in particular.

REFERENCES

Adrian, R.J., 2007, "Hairpin vortex organization in wall turbulence," *Phys. Fluids*, Vol. 19, 041301.

Del Alamo, J.C. and Jimenez, J., 2009, "Estimation of turbulent convection velocities and corrections to Taylor's approximation," *J. Fluid Mech.*, Vol. 640, pp. 5-26.

Bradshaw, P., 1967, "Inactive motion and pressure fluctuation in turbulent boundary layer," *J. Fluid Mech.*, Vol. 30, pp. 241-258.

Christensen, K.T. and Adrian, R.J., 2001, "Statistical evidence of hairpin vortex packets in wall turbulence," *J. Fluid Mech.*, Vol. 431, pp. 433-443.

Dennis, D.J. and Nickels, T.B., 2008, "On the limitations of Taylor's hypothesis in constructing long structures in a turbulent boundary layer," *J. Fluid Mech.*, Vol. 614, pp. 197-206.

Elsinga, G.E., Adrian, R.J., van Oudheusden, B.W. and Scarano, F., 2010, "Three-dimensional vortex organization in a high-Reynolds-number supersonic turbulent boundary layer," *J. Fluid Mech*., Vol. 644, pp. 35-60.

Elsinga, G.E. and Marusic, I., 2010, "Evolution and lifetimes of flow topology in a turbulent boundary layer," *Phys. Fluids*, Vol. 22, 015102.

Elsinga, G.E., Scarano, F., Wieneke, B. and Van Oudheusden, B.W., 2006, "Tomographic particle image velocimetry," *Exp. Fluids*, Vol. 41, pp. 933-947.

Guezennec, Y.G., Piomelli U. and Kim, J., 1989, "On the shape and dynamics of wall structures in turbulent channel flow," *Phys. Fluids A*, Vol. 1, pp. 764-766.

Kim, K.C. and Adrian, R.J., 1999, "Very large-scale motion in the outer layer," *Phys. Fluids*, Vol. 11, pp. 417-422.

Kim, J. and Hussain, F., 1993, "Propagation velocity of pertubations in turbulent channel flow," *Phys. Fluids A*, Vol. 3, pp. 695-706.

Krogstad, P.A., Kaspersen, J.H. and Rimestad, S., 1998, "Convection velocities in a turbulent boundary layer," *Phys. Fluids*, Vol. 10, pp. 949-957.

Lüthi, B., Tsinober, A. and Kinzelbach, W., 2005, "Lagrangian measurements of vorticity dynamics in turbulent flow," *J. Fluid Mech.*, Vol. 528, pp. 87-118.

Moin, P., 2009, "Revisiting Taylor's hypothesis," *J. Fluid Mech.*, Vol. 640, pp. 1-4.

Schröder, A., Geisler, R., Staack, K., Elsinga, G.E., Scarano, F., Wieneke, B., Henning, A., Poelma, C. and Westerweel, J., 2011, "Eulerian and Lagrangian views of a turbulent boundary layer flow using time-resolved tomographic PIV," *Exp. Fluids*, Vol. 50, pp. 1071-1091.

Taylor, G.I., 1921, "Diffusion by continous movements," *Proc. London Math. Soc.*, Vol. 20, pp. 196-202.

Taylor, G.I., 1938, "The spectrum of turbulence," *Proc. R. Soc. Lond.*, Vol. 164, pp. 476-490.

Tennekes, H., 1979, "The exponential Lagrangian correlation function and turbulent diffusion in the inertial subrange," *Atm. Env.*, Vol. 13, pp. 1565-1567.

Willmarth, W.W. and Wooldridge, C.E., 1962, "Measurements of the fluctuating pressure at the wall beneath a thick turbulent boundary layer," *J. Fluid Mech.*, Vol. 14, pp. 187-210.

Wills, J.A.B., 1964, "On convection velocities in turbulent shear flows," *J. Fluid Mech*., Vol. 20, pp. 417-432.